ACS APPLIED MATERIALS & INTERFACES

Research Article

Cite This: ACS Appl. Mater. Interfaces 2018, 10, 17942−17949

www.acsami.org

One-Dimensional $Cu_{2-x}Se$ Nanorods as the Cathode Material for High-Performance Aluminum-Ion Battery

Jiali Jiang,[†,∥] He Li,[†,∥] Tao Fu,[†] Bing-Joe Hwang,[‡] Xue Li,[*,§] and Jinbao Zhao[*,†]

[†]State Key Laboratory of Physical Chemistry of Solid Surfaces, Collaborative Innovation Center of Chemistry for Energy Materials, State-Province Joint Engineering Laboratory of Power Source Technology for New Energy Vehicle, College of Chemistry and Chemical Engineering, Xiamen University, No. 422 Siming South Road, Xiamen, Fujian 361005, China

[‡]Nano Electrochemistry Laboratory, Department of Chemical Engineering, National Taiwan University of Science and Technology, Taipei 106, Taiwan

[§]National and Local Joint Engineering Laboratory for Lithium-ion Batteries and Materials Preparation Technology, Key Laboratory of Advanced Battery Materials of Yunnan Province, Faculty of Metallurgical and Energy Engineering, Kunming University of Science and Technology, No. 68 Wenchang Road, Kunming, Yunnan 650093, China

Supporting Information

ABSTRACT: In this work, nonstoichiometric $Cu_{2-x}Se$ fabricated by a facile water evaporation process is used as high-performance Al-ion battery cathode materials. $Cu_{2-x}Se$ electrodes show high reversible capacity and excellent cycling stability, even at a high current density of 200 mA g^{-1}, the specific charge capacity in the initial cycle is 241 mA h g^{-1} and maintains 100 mA h g^{-1} after 100 cycles with a Coulombic efficiency of 96.1%, showing good capacity retention. The prominent kinetics of $Cu_{2-x}Se$ electrodes is also revealed by the GITT, which is attributed to the ultrahigh electronic conductivity of the $Cu_{2-x}Se$ material. Most importantly, an extensive research is dedicated to investigating the detailed intercalation and de-intercalation of relatively large chloroaluminate anions into the cubic $Cu_{2-x}Se$, which is conducive to better understand the reaction mechanism of the Al/$Cu_{2-x}Se$ battery.

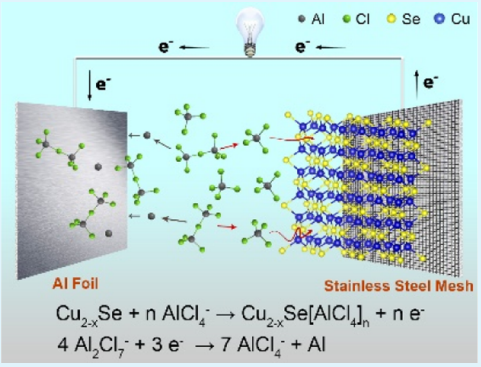

KEYWORDS: *one-dimensional nanorods, $Cu_{2-x}Se$, aluminum-ion battery, cathode material, reaction mechanism*

INTRODUCTION

In recent decades, lithium ion batteries (LIBs) have grown rapidly and been recognized as one of the most promising system for electrochemical energy storage because they have long cycle life, high energy density and no memory effect.[1,2] However, the scarcity of lithium sources caused by widespread application of LIBs and consequent safety concerns resulted from using combustible carbonates as electrolytes have turned current research focus toward high safety, cost-effective, and being environmental-friendly beyond-LIBs systems.[3−5]

Aluminum-ion batteries (AIBs) have lately aroused great concern among researchers because aluminum owns advantages including rich reserves, low cost, unrestricted distribution, and high stability compared with lithium.[6] Moreover, Al can transmit three electrons during the redox reaction and provide ultrahigh volumetric capacity (8.05 A h cm^{-3}), which is roughly fourfold and twofold greater than that of monovalent lithium (2.06 A h cm^{-3}) and divalent magnesium (3.83 A h cm^{-3}), respectively.[7] Al-storage cathode materials, as a significant component of rechargeable AIBs, have sparked heated discussions and extensive coverage over these years. A variety of novel cathode materials have been explored, including graphitic materials (natural graphite,[8] graphitic foam,[9] and graphene[10−12]), transitional metal oxides (V_2O_5[13] and TiO_2[14]), and chalcogenides (S,[15] CuS,[16] Ni_3S_2,[17] SnS_2,[18] and Mo_6S_8[19]). Transitional metal chalcogenides show great advantage in electrochemical capacity compared with other materials. For example, the specific capacities of Ni_3S_2 (350 mA h g^{-1}) and SnS_2 (392 mA h g^{-1}) in the initial discharge process outperform other cathode materials.[17,18] Recently, Wang and coworkers designed Co_9S_8@CNT−CNF as the electrode material for AIBs, which exhibits an ultrahigh specific discharge capacity of 315 mA h g^{-1} and extraordinary cyclic stability (maintains 87 mA h g^{-1} after 6000 cycles).[20] Hence, exploring novel metal chalcogenides as cathode electrodes has a profound impact on the future development of rechargeable AIBs.

In contrast with other metal chalcogenides, nonstoichiometric $Cu_{2-x}Se$ exhibits a unique crystal structure and material properties. The ball-and-stick model of $Cu_{2-x}Se$ is demonstrated in Figure 1b, a rigid face-centered cubic lattice consists of Se atoms in the material structure, while Cu ions are disorderly distributed around Se atoms with a high mobility.[2] The ultrahigh mobility of copper ions enables $Cu_{2-x}Se$ to be a distinguished p-type conductor and its electronic conductivity is

Received: February 25, 2018
Accepted: May 2, 2018
Published: May 2, 2018

DOI: 10.1021/acsami.8b03259
ACS Appl. Mater. Interfaces 2018, 10, 17942−17949

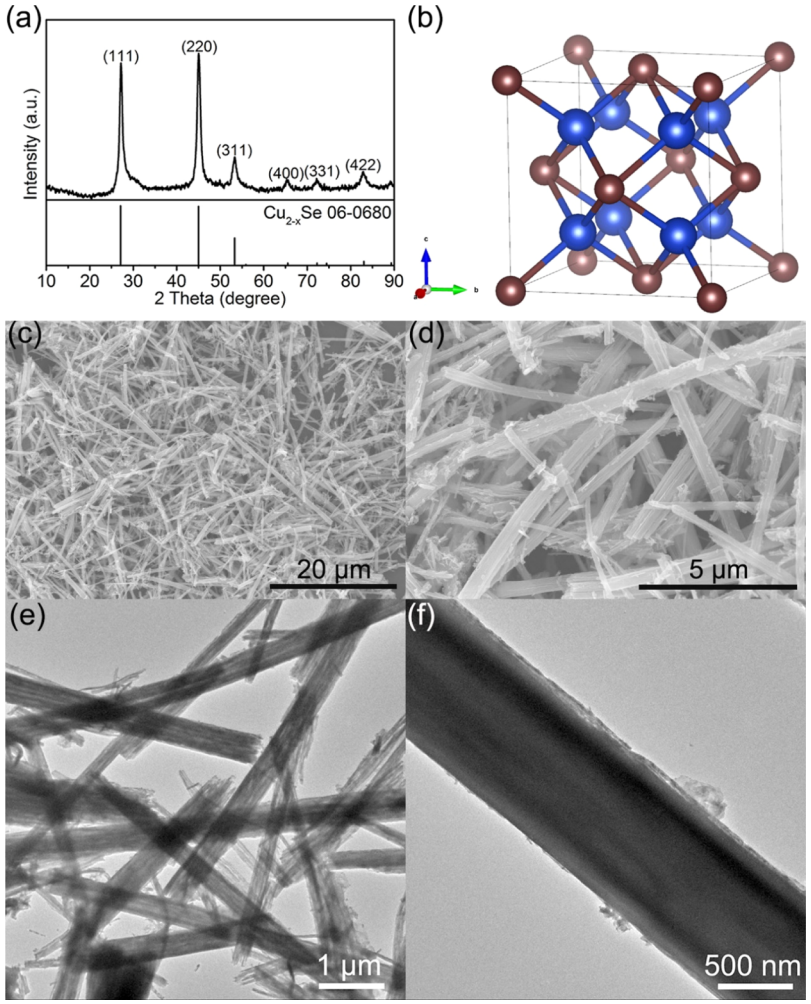

Figure 1. Physical characterizations of as-synthesized $Cu_{2-x}Se$ sample. (a) XRD pattern of $Cu_{2-x}Se$ powder. (b) Ball-and-stick model of $Cu_{2-x}Se$. Color code: Cu, blue; Se, brown. (c,d) SEM images and (e,f) TEM images of $Cu_{2-x}Se$ powder.

over 3000 times than that of the stoichiometric Cu_2Se.[21] Moreover, compared with CuS, $Cu_{2-x}Se$ has a much larger cell volume (189 $Å^3$), which can better accommodate the intercalation and de-intercalation of chloroaluminate ions, resulting in higher specific capacity and better cycle performance. Besides, the one-dimensional structure can not only preferably accommodate the volume change during repeated insertion/extraction but also increase the contact area with electrolyte and decrease the ion diffusion length, which are conducive to fast charge transfer.[22−25] To sum up, the one-dimensional $Cu_{2-x}Se$ nanorod material is an eligible cathode material candidate for the rechargeable AIBs.

Herein, we first report the one-dimensional $Cu_{2-x}Se$ nanorod material as a promising cathode for AIBs with acidic ionic liquid as the electrolyte. It is revealed that the ultrahigh electronic conductivity, large cell volume, and one-dimensional structure lead to outstanding electrochemical properties of $Cu_{2-x}Se$ electrodes in AIBs. At 50 mA g^{-1}, the specific charge capacity and discharge capacity in the initial cycle are 277 and 260 mA h g^{-1}, respectively, with a Coulombic efficiency (CE) of 93.9%. Even at a much higher current density of 200 mA g^{-1}, the specific charge capacity in the initial cycle is 241 mA h g^{-1} and maintains 100 mA h g^{-1} after 100 cycles with a CE of 96.1%, showing good capacity retention. The diffusion coefficients of aluminum ions at various charging and discharging states fall in between 6.19×10^{-16} and 9.94×10^{-12} cm^2 s^{-1}, which are superior to other metal chalcogenides, demonstrating the prominent kinetics of the $Cu_{2-x}Se$ material. Moreover, intensive investigations have been implemented to confirm the electrochemical reaction processes occurring in the $Cu_{2-x}Se$/Al battery. This work not only introduces a high-performance cathode for rechargeable AIBs but also enriches the in-depth understanding of the charge/discharge reaction mechanism.

RESULTS AND DISCUSSION

Material Characterization. The sample compositions of as-prepared $Cu_{2-x}Se$ were surveyed by X-ray diffraction (XRD), and the achieved XRD pattern is illustrated in Figure 1a. The diffraction lines are in accordance with the powder diffraction file (PDF) card of cubic $Cu_{2-x}Se$ (space group: $F\bar{4}3m$) (PDF no. 06-0680, JCPDS, 2004), several intensive diffraction peaks at 26.7°, 44.6°, and 52.9° agree well with (111), (220), and (311) planes of cubic $Cu_{2-x}Se$, respectively, and no impure diffraction line can be detected, demonstrating high purity of as-synthesized $Cu_{2-x}Se$. The X-ray photoelectron spectroscopy (XPS) survey spectrum (Figure S1) of $Cu_{2-x}Se$ electrode (before electrochemical tests) affirms the coexistence of Cu, Se, C, and O, where O is attributed to the sample exposed to the air, and the appearance of C is due to acetylene black in the

DOI: 10.1021/acsami.8b03259
ACS Appl. Mater. Interfaces 2018, 10, 17942−17949

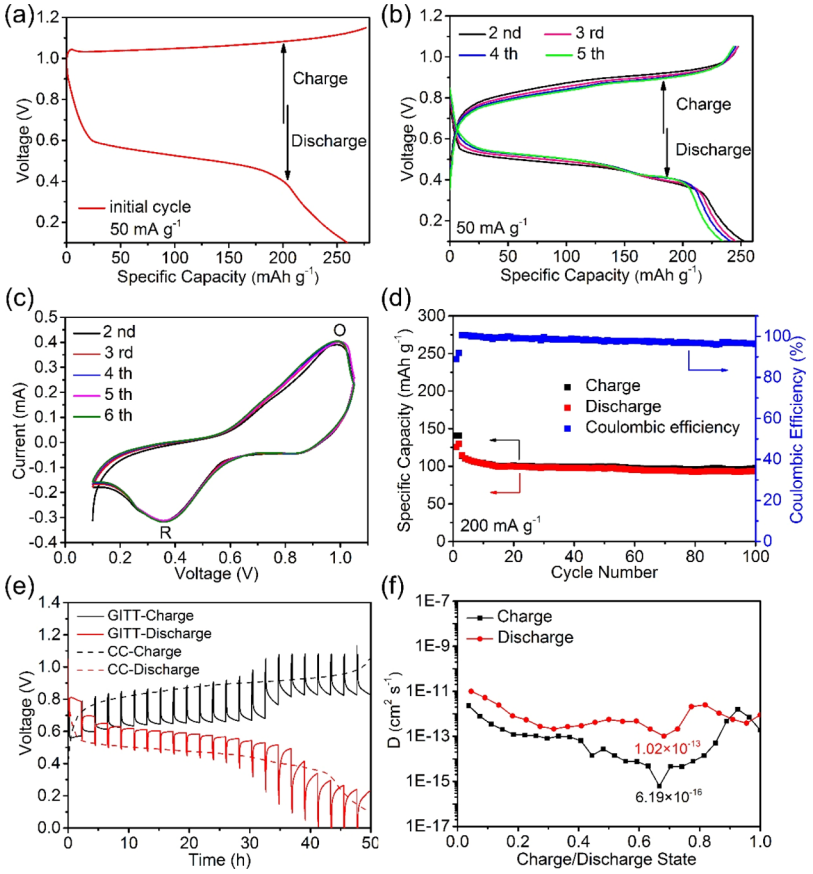

Figure 2. Electrochemical characterizations of Al/$Cu_{2-x}Se$ cells at room temperature (25 °C). (a) Charge/discharge curves in the first cycle at 50 mA g^{-1}. (b) Galvanostatic electrochemical curves from the second to the fifth cycle. (c) Cyclic voltammograms at 0.2 mV s^{-1}. (d) Cycling performance with CE at 200 mA g^{-1}. (e) Galvanostatic intermittent titration technique (GITT) curve and constant current (CC) curve at 50 mA g^{-1}. (f) Calculated aluminum ion diffusion coefficients from GITT curves.

$Cu_{2-x}Se$ electrode. The scanning electron microscopy (SEM) and transmission electron microscopy (TEM) tests were carried out to analyze the morphology of $Cu_{2-x}Se$ powder. As illustrated in Figure 1c,d, the diameter of $Cu_{2-x}Se$ nanorods ranges from 300 to 800 nm and can reach tens of micrometers in length. TEM images in Figure 1e,f state that $Cu_{2-x}Se$ nanorods with a uniform diameter are bundled together by many thin nanowires. Figure S2 displays the elemental distribution of $Cu_{2-x}Se$ powder, where Cu and Se elements are distributed evenly in $Cu_{2-x}Se$ nanorods. Normalized content of Cu and Se elements is revealed in Table S1, the atomic ratio of Cu to Se is about 1.84; hence, the x value calculated by the energy-dispersive spectroscopy (EDS) test is roughly 0.16, which is in accordance with previous reports.[2,26]

Electrochemical Performance. Figure 2a,b exhibits the galvanostatic electrochemical curves at 50 mA g^{-1}, the charge and discharge capacities in the first cycle are 277 and 260 mA h g^{-1}, respectively, with a CE of 93.9%. The irreversible capacity loss is due to the probability that Al is sunk into the frame structure of cubic $Cu_{2-x}Se$ and cannot provide capacity in the discharge process.[27] The completely overlapped charge/discharge curves of Figure 2b illustrate the excellent cycle stability of $Cu_{2-x}Se$ electrodes in AIBs. The specific charge/discharge capacities are 247 and 252 mA h g^{-1} in the second cycle. From the third to the fifth cycle, the specific charge capacities maintain in 247, 245, and 244 mA h g^{-1} with the relevant CE of 99.3, 98.1, and 96.2%, respectively. Furthermore, the overlapped charge and discharge plateaus in electrochemical curves locate at 0.9 and 0.5 V (vs $Al/AlCl_4^-$), corresponding to the oxidation process and reduction process occurring in the $Cu_{2-x}Se$ electrode, respectively. When the current density increases to 100 mA g^{-1}, the specific charge capacities of initial three cycles (Figure S3a) are 271, 256, and 244 mA h g^{-1}, respectively, and the charge and discharge capacities are 174 and 162 mA h g^{-1} with a capacity retention of 70.8% after 30 cycles (Figure S3c). Even at 200 mA g^{-1}, the initial charge capacity is still as high as 241 mA h g^{-1}, and the charge capacity decreases to 176 mA h g^{-1} in the fifth cycle (Figure S3b). The cyclic performance along with CE after the activation process (Figure S3b) is illustrated in Figure 2d; after 100 cycles, the $Cu_{2-x}Se$ electrode exhibits a highly reversible capacity of about 100 mA h g^{-1} and the CE is nearly 96.1%. Cyclic voltammograms (Figure 2c) were also tested at a scan rate of 0.2 mV s^{-1}. A pair of distinct oxidation peak (O) and reduction peak (R) exist at around 0.99 and 0.36 V versus $Al/AlCl_4^-$, which are in accord with the charge and discharge platforms. Besides, overlapped cyclic voltammetry (CV) curves declare the outstanding reversibility of $Cu_{2-x}Se$ material in rechargeable AIBs. The rate performance of Al/$Cu_{2-x}Se$ battery at different current densities from 100 to 500 mA g^{-1} is illustrated in Figure S3d. At 100, 200, and 500 mA g^{-1}, the specific charge capacities are 247, 201, and 104 mA h g^{-1}, respectively. After reducing the current density to 100 mA g^{-1}, the specific charge capacity can go back to 190 mA h g^{-1} with the CE of 98.7%, which indicates the prominent rate capability of the $Cu_{2-x}Se$ material. The electronic conductivities of $Cu_{2-x}Se$ and CuS powder were

DOI: 10.1021/acsami.8b03259
ACS Appl. Mater. Interfaces 2018, 10, 17942−17949

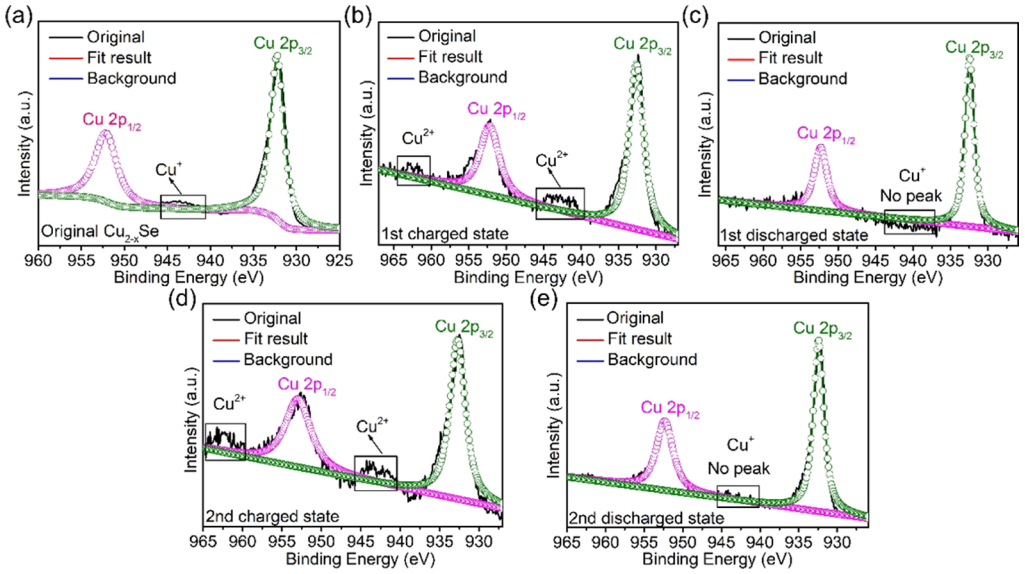

Figure 3. XPS Cu 2p spectra during different electrochemical states. (a) Pristine $Cu_{2-x}Se$ electrode. (b) First charged state. (c) First discharged state. (d) Second charged state. (e) Second discharged state.

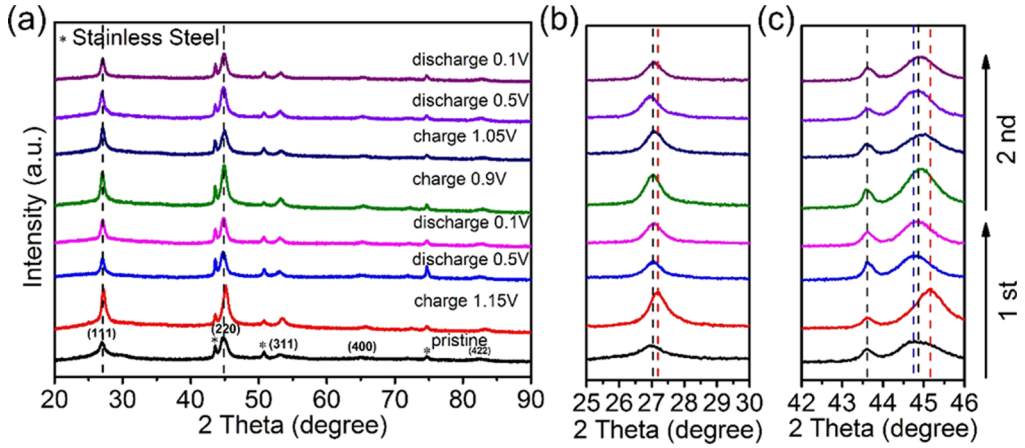

Figure 4. (a) XRD patterns collected at various charging and discharging conditions. (b) Enlarged view of selected region (25−30°). (c) Enlarged view of selected region (42−46°).

tested by four-probe conductivity measurements, the specific conductivity of $Cu_{2-x}Se$ is 340 S cm^{-1}, which is much larger than that of CuS (42 S cm^{-1}). The impressive electronic conductivity plays a significant part in the prominent rate performance of $Cu_{2-x}Se$ electrode. In summary, $Cu_{2-x}Se$ electrodes reveal the superb cycle stability and rate capability, and the superiority of electrochemical performance resulted from the ultrahigh electronic conductivity and larger crystal cell volume of $Cu_{2-x}Se$.[28]

The GITT measurements were executed to investigate the kinetics of $Cu_{2-x}Se$ electrodes. In a typical GITT test, the Al/$Cu_{2-x}Se$ battery was cycled five times at 50 mA g^{-1} in advance. Subsequently, battery charged and discharged by a current impulse at 50 mA g^{-1} for 600 s (τ) and stood for 2 h with no current impulse; the above procedures were repeated several times. Figure 2e demonstrates the GITT curve and CC curve of $Cu_{2-x}Se$ electrodes in the charge and discharge processes. The charge plateau and discharge plateau in the GITT curve are around 0.9 and 0.5 V, which are also observed in the CC curve. The diffusion coefficients of aluminum ions in $Cu_{2-x}Se$ electrodes can be calculated from the GITT data by eq 1.[29−31]

$$D \approx \frac{4}{\pi\tau}\left(\frac{mV_m}{zMA}\right)^2\left(\frac{\Delta E_s}{\Delta E_\tau}\right)^2 \qquad \left(\tau \ll \frac{L^2}{D}\right) \tag{1}$$

In this equation, the molar volume (cm^3 mol^{-1}) is represented as V_m, z stands for the charge number, A is effective surface area (cm^2) of $Cu_{2-x}Se$ electrode, E_s is steady-state potential (V) measured during the rest time, E_τ is the potential (V) measured during the current pulse of duration τ (s), M and m are the molecular mass (g mol^{-1}) and mass of the active material, respectively, and L is the thickness of the electrode (cm).[32] ΔE_s is the change of steady-state voltage after a charge or discharge process and standing, and ΔE_τ is the potential change after a charge or discharge process.[33,34] The test results are demonstrated in Figure 2f, Al-ion diffusion coefficients of the electrode material during different charging processes lie in 6.19×10^{-16} to 2.31×10^{-12} cm^2 s^{-1} and range from 1.02×10^{-13} to 9.94×10^{-12} cm^2 s^{-1} in the discharge process, which are well above that of other metal chalcogenides, such as Mo_6S_8 (10^{-17} to 10^{-19} cm^2 s^{-1}).[30] The prominent kinetics of $Cu_{2-x}Se$ can be ascribed to its ultrahigh electronic conductivity and one-dimensional nanorod structure.[21] In

DOI: 10.1021/acsami.8b03259
ACS Appl. Mater. Interfaces 2018, 10, 17942−17949

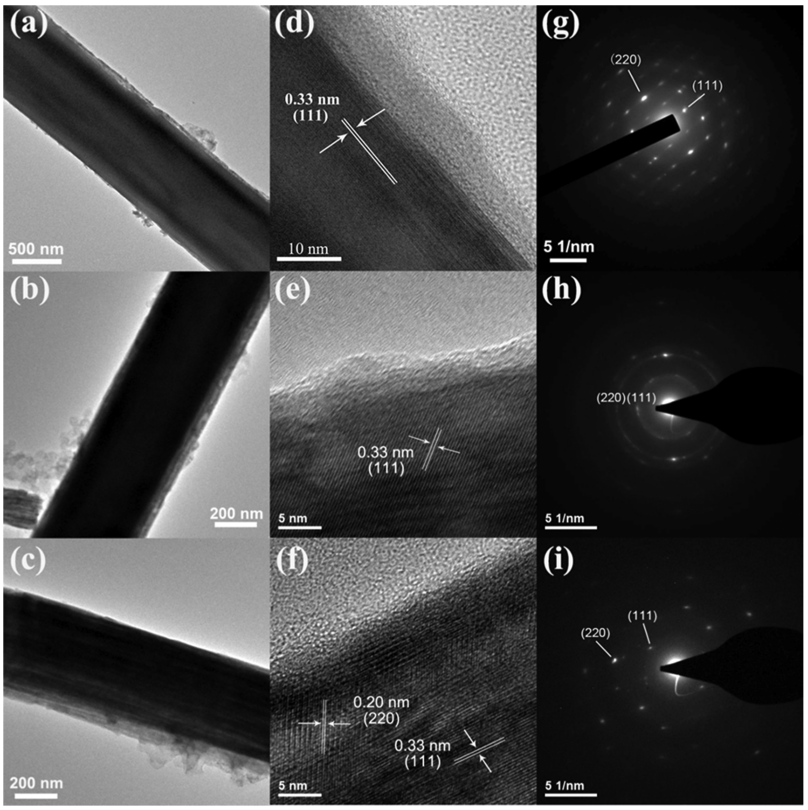

Figure 5. (a–c) TEM images of original $Cu_{2-x}Se$, charged state, discharged state in the initial cycle, respectively. (d–f) HRTEM images corresponding to (a–c). (g–i) SAED patterns corresponding to (a–c).

addition, the aluminum ion diffusion coefficients during the discharge process are much higher than that in the charge process, suggesting that the insertion of $AlCl_4^-$ into the structure of $Cu_{2-x}Se$ is harder than extraction process.

Electrochemical Reaction Mechanism. The Al 2p spectra and Cl 2p spectra of $Cu_{2-x}Se$ electrodes in the second cycle are revealed in the Figure S5a,b. It is shown that aluminum and chlorine content are increasing with the increased charging depth and reducing with the increased discharging depth, affirming the reversible storage of polyanions $AlCl_4^-$ in $Cu_{2-x}Se$ electrodes.[35] Se 3d spectra during different charge and discharge processes (Figure S6a–e) are very analogous and consistent, demonstrating a stable valence state of selenium element during the whole electrochemical process, hence copper is the main element with varied valence to equilibrate charges during the intercalation/de-intercalation process of $AlCl_4^-$. Cu 2p spectra during the initial two cycles are exhibited in Figure 3a–e, for the original $Cu_{2-x}Se$ electrode, two strong peaks located at 932.2 and 952.2 eV stand for Cu $2p_{3/2}$ and Cu $2p_{1/2}$.[22,36] At about 943.6 eV, there is a minimal satellite peak representing Cu^+,[16] then the stronger satellite peak at the initial charged state reveals the existence of Cu^{2+}.[37,38] In the light of the charge/discharge mechanism of $Cu_{2-x}Se$ electrodes, it can be inferred the insertion of $AlCl_4^-$ ions into the cubic $Cu_{2-x}Se$ will be companied by the oxidation of Cu^+. In the following discharged state, the disappearance of satellite peak around 943.6 eV manifests the reduction reaction of Cu^{2+} to Cu^+.[39,40] The identical trend is also observed in the second cycle. The above results further illuminate the electrochemical reversibility of $Cu_{2-x}Se$ electrodes upon the insertion and extraction of $AlCl_4^-$ ions.

To solidly deepen the understanding of structural reversibility of $Cu_{2-x}Se$ nanorods upon the charge/discharge process, ex situ XRD measurements during the initial two charge/discharge cycles were performed with the scan rate of 2° min^{-1}, as indicated in Figure 4a. Two intensive diffraction peaks at 27.02° and 44.88° represent the (111) and (220) planes of cubic $Cu_{2-x}Se$ (PDF no. 06-0680, JCPDS, 2004), and these peaks with an asterisk represent the existence of stainless steel current collector. Significantly, no new peak can be found in XRD patterns at different charge/discharge states, indicating that $Cu_{2-x}Se$ may have no phase transformation. According to the enlarged view of Figure 4c, the diffraction peak at 43.60° which stands for stainless steel has no change in peak intensity and peak shift during the electrochemical reaction, which demonstrates the validity and credibility of ex situ XRD patterns at different insertion and deinsertion states. The diffraction peak in Figure 4b, which represents the (111) plane, slightly shifts to a higher degree with the increased charge depth, and the displacement distance toward right is roughly 0.15°, showing the decrement of *d* space. The phenomenon is abnormal in intercalation electrodes for rechargeable batteries, which can be speculated that there is a slight volume shrinkage in the frame structure of the $Cu_{2-x}Se$ material. To some extent, the similar situation in Figure 4c is more apparent. The diffraction peak at 44.88° mildly shifts to a higher degree (45.16°) in the charge process and moves back to 44.86° in the subsequent discharge process. The same rule is also observed in the next cycle, indicating the structural reversibility of $Cu_{2-x}Se$ upon charge/discharge cycles. Furthermore, there is a tiny crystallization reduction after two cycles; the decrease of crystallinity and the displacement distance of diffraction peak are much more evident by comparing XRD patterns of $Cu_{2-x}Se$

DOI: 10.1021/acsami.8b03259
ACS Appl. Mater. Interfaces 2018, 10, 17942–17949

electrodes before and after 200 cycles (Figure S7a). The intensity of diffraction peak which represents the (220) plane declines sharply, whereas other peaks have no distinct change, suggesting that $AlCl_4^-$ ions are likely to pass through the (220) plane of cubic $Cu_{2-x}Se$ to participate in the electrochemical reaction. In Figure S7b, it is easily measured that the displacement distance of diffraction peak toward right is 0.21° compared with the pristine diffraction peak. On the basis of the above results, some conclusions can be obtained. The material structure will slightly distort to accommodate the intercalation of $AlCl_4^-$ and then slowly rehabilitate along with the extraction of $AlCl_4^-$, in other words, the structural change of every cycle is a quasireversible process. Moreover, the crystallinity decrement of $Cu_{2-x}Se$ electrodes is an accumulating process upon the repeated insertion and extraction of $AlCl_4^-$, and the irreversible deterioration of the crystal structure mainly leads to the capacity fading of $Cu_{2-x}Se$ electrodes. A similar phenomenon also occurs in AIBs with other materials as cathodes.[27]

The morphology and composition characterizations of $Cu_{2-x}Se$ electrodes during the different electrochemical processes have also been demonstrated in Figure 5. It is particularly noted that the morphology of nanorods can be well-maintained. The corresponding high-resolution TEM (HRTEM) figures and selected area electron diffraction (SAED) patterns are indicated in Figure 5d–i, the lattice fringe spacing of 0.33 nm in original $Cu_{2-x}Se$ electrode perfectly matches the interplanar spacing of (111) plane of cubic $Cu_{2-x}Se$.[32] The relevant SAED pattern describes that $Cu_{2-x}Se$ nanorods are single crystal structure, these diffraction spots match well with (111) and (220) planes of cubic $Cu_{2-x}Se$.[26] The distinct lattice fringes after the initial charge process indicate decent crystallinity of $Cu_{2-x}Se$ to some extent, but the SAED rings in Figure 5h manifest the material crystallization reduced slightly. The mapping images of fully charged $Cu_{2-x}Se$ electrode are shown in Figure S8, the distribution of Cu, Se, Al, and Cl elements overlaps in $Cu_{2-x}Se$ nanorods, indicating the intercalation of $AlCl_4^-$ into the unit cell of $Cu_{2-x}Se$. As demonstrated in Figure 5f–i, the interplanar spacing of 0.20 and 0.33 nm are indexed to (220) and (111) planes, respectively, and blurry diffraction spots also agree well with (220) and (111) planes, suggesting the crystallographic recovery of $Cu_{2-x}Se$.[41] Figure S9 reveals the morphology information of $Cu_{2-x}Se$ after 200 charge/discharge cycles, showing a slight collapse that occurred in the material structure and the material crystallization reduced greatly after long cycling, which is consistent with the XRD result (Figure S7).

The changes in ionic compositions and ion concentrations of acidic ionic liquid during different charge/discharge processes were also obtained by ^{27}Al nuclear magnetic resonance (NMR) spectra, which is important for further exploring the detailed electrochemical reactions occurring in Al/$Cu_{2-x}Se$ battery system. In Figure 6, two peaks at 103.95 and 98.15 ppm can be attributed to the $AlCl_4^-$ and $Al_2Cl_7^-$ ions.[42] It is demonstrated that $Al_2Cl_7^-$ ions and $AlCl_4^-$ ions are both main components in electrolyte at different states, and their concentrations vary with different charge/discharge processes. The molar proportion of $AlCl_4^-$ ions to $Al_2Cl_7^-$ ions can be calculated by multi-peak-fitting and integrating process; the computed result was 3.13:1 in the pristine electrolyte. Subsequently, it decreased to nearly 1.48:1 after the initial charge process, and the molar ratio increased to 2.14:1 at the initial discharge state, further confirming the intercalation and

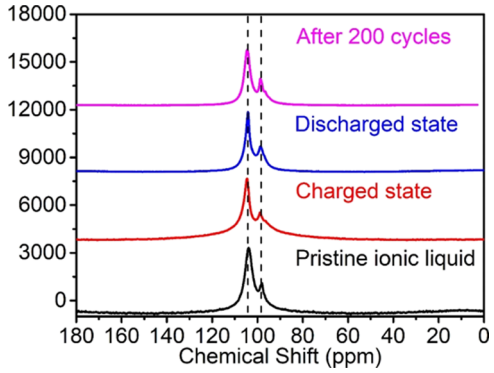

Figure 6. ^{27}Al NMR spectra of electrolyte at different electrochemical states.

de-intercalation of $AlCl_4^-$ in cubic $Cu_{2-x}Se$.[5,17] Particularly, the molar ratio reduced to 1.78:1 after 200 cycles, which is far below that of the pristine electrolyte, showing the irreversible loss of $AlCl_4^-$ ions in acidic liquid, and this may be another reason for the capacity loss of $Cu_{2-x}Se$ electrodes after long cycling.

On the basis of the above results, the simplified electrochemical reaction process of Al/$Cu_{2-x}Se$ battery during charging and discharging can be formulated as

$$Cu_{2-x}Se + nAlCl_4^- \rightleftharpoons Cu_{2-x}Se[AlCl_4]_n + ne^- \quad (2)$$

$$4Al_2Cl_7^- + 3e^- \rightleftharpoons 7AlCl_4^- + Al \quad (3)$$

In the $Cu_{2-x}Se$ electrode, primarily $AlCl_4^-$ ions are intercalated and de-intercalated in the $Cu_{2-x}Se$ material at various charging and discharging conditions. In the Al electrode, complex $Al_2Cl_7^-$ ions are decomposed into $AlCl_4^-$ and Al^{3+} in the charge process, and Al^{3+} will simultaneously deposit in aluminum anode, whereas the opposite reactions occur when discharging. It is speculated that $Al_2Cl_7^-$ ions have electrochemical activity in AIBs, and the redox reactions rely on the interconversion between $Al_2Cl_7^-$ and $AlCl_4^-$, which is the main reason why acidic ionic liquid is chosen as electrolyte for AIBs. Figure 7 is the schematic illustration of Al/$Cu_{2-x}Se$ cell.

CONCLUSION

In conclusion, it is the first time that $Cu_{2-x}Se$ is reported as the cathode material for rechargeable AIBs. The $Cu_{2-x}Se$ material exhibits a high specific capacity and excellent cycling stability.

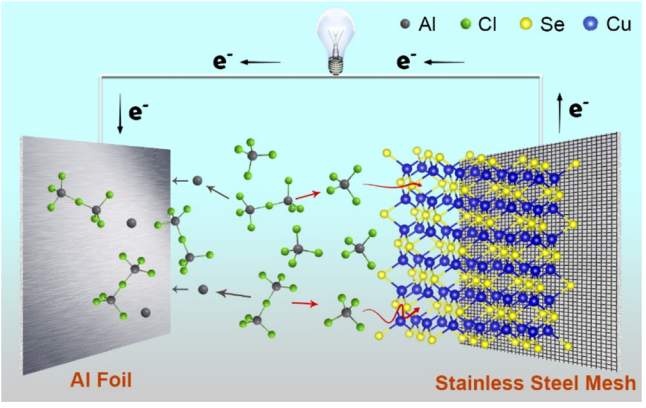

Figure 7. Schematic illustration of the Al/$Cu_{2-x}Se$ cell.

DOI: 10.1021/acsami.8b03259
ACS Appl. Mater. Interfaces 2018, 10, 17942–17949

At 50 mA g^{-1}, the charge/discharge capacities in the initial cycle are 277 and 260 mA h g^{-1} and the CE is 93.9%. Even at a much higher current density of 200 mA g^{-1}, the $Cu_{2-x}Se$ electrode indicates a high charge capacity of 241 mA h g^{-1} in the initial cycle and maintains a reversible capacity of over 100 mA h g^{-1} after 100 cycles with the CE of 96.1%. The prominent electrochemical performance is ascribed to its ultrahigh electronic conductivity, the large enough cell volume, and one-dimensional structure. Besides, the detailed electrochemical reactions occurring in the Al/$Cu_{2-x}Se$ cell also have been intensively investigated. XPS Al 2p spectra and Cl 2p spectra affirm the reversible insertion of polyanions $AlCl_4^-$ in $Cu_{2-x}Se$ material. The XRD pattern after 200 cycles suggests $AlCl_4^-$ ions may pass through (220) plane of cubic $Cu_{2-x}Se$ to take part in the electrochemical reactions, and the irreversible deterioration of crystal structure is the main reason why the specific capacity of Al/$Cu_{2-x}Se$ cell fade greatly after long cycling. ^{27}Al NMR spectra indicate the redox reactions depend on the conversion between $AlCl_4^-$ and $Al_2Cl_7^-$ ions in the electrolyte. To sum up, the one-dimensional $Cu_{2-x}Se$ electrode material has high capacity, cost-effectiveness and high safety, which provides an ideal choice for future AIBs.

EXPERIMENTAL SECTION

Preparation of One-Dimensional $Cu_{2-x}Se$ Nanorods. $Cu_{2-x}Se$ materials were fabricated by a facile water evaporation process, the detailed preparation method of the $Cu_{2-x}Se$ material can be referred to the experimental section of our previous publication.[32]

Synthesis of Electrolyte for AIBs. Prior to synthesis, 1-ethyl-3-methylimidazolium chloride ([EMIm]Cl, 98%, Aladdin) and aluminum chloride anhydrous ($AlCl_3$, 99%, Aladdin) were separately heated at 130 °C in vacuum oven for 12−16 h to remove residual moisture. AIB electrolyte was synthesized by slowly adding a certain amount of $AlCl_3$ powder into [EMIm]Cl at 130 °C with the optimal molar proportion of 1.3, and the resulting transparent light-yellow solution was mixed under magnetical stirring for a few hours and then stood for no less than 12 h. The synthesis of the electrolyte was manipulated in the absence of water and oxygen.

Electrochemical Measurements. Soft package AIBs were assembled to measure the electrochemical characteristics of the as-prepared $Cu_{2-x}Se$ nanorods and the cell size is 1 cm × 1 cm. The fabrication method of the positive plate is as follows: 70 wt % $Cu_{2-x}Se$ material, 20 wt % acetylene black, and 10 wt % polytetrafluoroethylene binder were dispersed in absolute ethanol as slurry and then coated it on the 1 cm^2 stainless steel current collector, and positive plates were subsequently dried in a vacuum drying oven at 60 °C for more than 10 h to get rid of residual ethanol. Soft package AIBs were all prepared in the absence of water and oxygen. The CC electrochemical performance tests and GITT tests were implemented on the Neware battery test system. CV measurement was executed on the CHI 660D potentiostat.

Characterization Techniques. Rigaku Ultima IV diffractometer was employed to obtain the XRD data. Hitachi S-4800 was applied to get the SEM and EDS data of $Cu_{2-x}Se$ material. Tecnai F30 was used to acquire the morphology of $Cu_{2-x}Se$ electrodes at various charging and discharging conditions; corresponding SAED patterns and EDS mapping tests were also conducted on Tecnai F30. A PHI Quantum 2000 scanning ESCA microprobe was operated to measure the XPS spectra. Bruker AVANCE II 400 spectrometer was executed to measure ^{27}Al NMR spectra of electrolytes. ST-2722 semiconductor resistivity of the powder tester was used to test the conductivity of as-prepared material.

ASSOCIATED CONTENT

Supporting Information

The Supporting Information is available free of charge on the ACS Publications website at DOI: 10.1021/acsami.8b03259.

Electrochemical performance of $Cu_{2-x}Se$ electrodes and stainless steel mesh, XPS Al 2p spectra, Cl 2p spectra and Se 3d spectra at various charging and discharging conditions, XRD pattern of $Cu_{2-x}Se$ electrode after 200 cycles, and TEM and HRTEM figures of $Cu_{2-x}Se$ after 200 charge/discharge cycles (PDF)

AUTHOR INFORMATION

Corresponding Authors

*E-mail: lxcau@126.com (X.L.).
*E-mail: jbzhao@xmu.edu.cn (J.Z.).

ORCID

Jiali Jiang: 0000-0003-4578-813X
He Li: 0000-0002-5324-8101
Bing-Joe Hwang: 0000-0002-3873-2149
Jinbao Zhao: 0000-0002-2753-7508

Author Contributions

‖J.J. and H.L. make equal contributions and share the first authorship.

Notes

The authors declare no competing financial interest.

ACKNOWLEDGMENTS

This research work was financially supported by National Natural Science Foundation of China (nos. 21621091 and 51604132) and Provincial Natural Science Foundation of Yunnan (no. 2017FB085). We deeply appreciate the suggestions from Prof. Daiwei Liao in the revision of manuscript.

REFERENCES

(1) Yang, Y.; Zheng, G.; Misra, S.; Nelson, J.; Toney, M. F.; Cui, Y. High-Capacity Micrometer-Sized Li_2S Particles as Cathode Materials for Advanced Rechargeable Lithium-Ion Batteries. *J. Am. Chem. Soc.* **2012**, *134*, 15387−15394.

(2) Li, H.; Jiang, J.; Wang, F.; Huang, J.; Wang, Y.; Zhang, Y.; Zhao, J. Facile Synthesis of Rod-Like $Cu_{2-x}Se$ and Insight into its Improved Lithium-Storage Property. *ChemSusChem* **2017**, *10*, 2235−2241.

(3) Zafar, Z. A.; Imtiaz, S.; Razaq, R.; Ji, S.; Huang, T.; Zhang, Z.; Huang, Y.; Anderson, J. A. Cathode Materials for Rechargeable Aluminum Batteries: Current Status and Progress. *J. Mater. Chem. A* **2017**, *5*, 5646−5660.

(4) Elia, G. A.; Marquardt, K.; Hoeppner, K.; Fantini, S.; Lin, R.; Knipping, E.; Peters, W.; Drillet, J.-F.; Passerini, S.; Hahn, R. An Overview and Future Perspectives of Aluminum Batteries. *Adv. Mater.* **2016**, *28*, 7564−7579.

(5) Lin, M.-C.; Gong, M.; Lu, B.; Wu, Y.; Wang, D.-Y.; Guan, M.; Angell, M.; Chen, C.; Yang, J.; Hwang, B.-J.; Dai, H. An Ultrafast Rechargeable Aluminium-Ion Battery. *Nature* **2015**, *520*, 325−328.

(6) Das, S. K.; Mahapatra, S.; Lahan, H. Aluminium-Ion Batteries: Developments and Challenges. *J. Mater. Chem. A* **2017**, *5*, 6347−6367.

(7) Ambroz, F.; Macdonald, T. J.; Nann, T. Trends in Aluminium-Based Intercalation Batteries. *Adv. Energy Mater.* **2017**, *7*, 1602093.

(8) Wang, D.-Y.; Wei, C.-Y.; Lin, M.-C.; Pan, C.-J.; Chou, H.-L.; Chen, H.-A.; Gong, M.; Wu, Y.; Yuan, C.; Angell, M.; Hsieh, Y.-J.; Chen, Y.-H.; Wen, C.-Y.; Chen, C.-W.; Hwang, B.-J.; Chen, C.-C.; Dai, H. Advanced Rechargeable Aluminium Ion Battery with a High-Quality Natural Graphite Cathode. *Nat. Commun.* **2017**, *8*, 14283.

DOI: 10.1021/acsami.8b03259
ACS Appl. Mater. Interfaces 2018, 10, 17942−17949

(9) Yu, X.; Wang, B.; Gong, D.; Xu, Z.; Lu, B. Graphene Nanoribbons on Highly Porous 3D Graphene for High-Capacity and Ultrastable Al-Ion Batteries. *Adv. Mater.* **2017**, *29*, 1604118.
(10) Chen, H.; Xu, H.; Wang, S.; Huang, T.; Xi, J.; Cai, S.; Guo, F.; Xu, Z.; Gao, W.; Gao, C. Ultrafast All-Climate Aluminum-Graphene Battery with Quarter-Million Cycle Life. *Sci. Adv.* **2017**, *3*, No. eaao7233.
(11) Chen, H.; Guo, F.; Liu, Y.; Huang, T.; Zheng, B.; Ananth, N.; Xu, Z.; Gao, W.; Gao, C. A Defect-Free Principle for Advanced Graphene Cathode of Aluminum-Ion Battery. *Adv. Mater.* **2017**, *29*, 1605958.
(12) Zhao, X.; Yao, W.; Gao, W.; Chen, H.; Gao, C. Wet-Spun Superelastic Graphene Aerogel Millispheres with Group Effect. *Adv. Mater.* **2017**, *29*, 1701482.
(13) Wang, H.; Bi, X.; Bai, Y.; Wu, C.; Gu, S.; Chen, S.; Wu, F.; Amine, K.; Lu, J. Open-Structured $V_2O_5{\cdot}nH_2O$ Nanoflakes as Highly Reversible Cathode Material for Monovalent and Multivalent Intercalation Batteries. *Adv. Energy Mater.* **2017**, *7*, 1602720.
(14) Liu, S.; Hu, J. J.; Yan, N. F.; Pan, G. L.; Li, G. R.; Gao, X. P. Aluminum Storage Behavior of Anatase TiO_2 Nanotube Arrays in Aqueous Solution for Aluminum Ion Batteries. *Energy Environ. Sci.* **2012**, *5*, 9743−9746.
(15) Yang, H.; Yin, L.; Liang, J.; Sun, Z.; Wang, Y.; Li, H.; He, K.; Ma, L.; Peng, Z.; Qiu, S.; Sun, C.; Cheng, H.-M.; Li, F. An Aluminum-Sulfur Battery with a Fast Kinetic Response. *Angew. Chem., Int. Ed. Engl.* **2018**, *57*, 1898−1902.
(16) Wang, S.; Jiao, S.; Wang, J.; Chen, H.-S.; Tian, D.; Lei, H.; Fang, D.-N. High-Performance Aluminum-Ion Battery with CuS@C Microsphere Composite Cathode. *ACS Nano* **2017**, *11*, 469−477.
(17) Wang, S.; Yu, Z.; Tu, J.; Wang, J.; Tian, D.; Liu, Y.; Jiao, S. A Novel Aluminum-Ion Battery: Al/$AlCl_3$-[EMIm]Cl/Ni_3S_2@Graphene. *Adv. Energy Mater.* **2016**, *6*, 1600137.
(18) Hu, Y.; Luo, B.; Ye, D.; Zhu, X.; Lyu, M.; Wang, L. An Innovative Freeze-Dried Reduced Graphene Oxide Supported SnS_2 Cathode Active Material for Aluminum-Ion Batteries. *Adv. Mater.* **2017**, *29*, 1606132.
(19) Geng, L.; Lv, G.; Xing, X.; Guo, J. Reversible Electrochemical Intercalation of Aluminum in Mo_6S_8. *Chem. Mater.* **2015**, *27*, 4926−4929.
(20) Hu, Y.; Ye, D.; Luo, B.; Hu, H.; Zhu, X.; Wang, S.; Li, L.; Peng, S.; Wang, L. A Binder-Free and Free-Standing Cobalt Sulfide@Carbon Nanotube Cathode Material for Aluminum-Ion Batteries. *Adv. Mater.* **2018**, *30*, 1703824.
(21) Liu, H.; Shi, X.; Xu, F.; Zhang, L.; Zhang, W.; Chen, L.; Li, Q.; Uher, C.; Day, T.; Snyder, G. J. Copper Ion Liquid-Like Thermoelectrics. *Nat. Mater.* **2012**, *11*, 422−425.
(22) Chen, X.; Li, Z.; Yang, J.; Sun, Q.; Dou, S. Aqueous Preparation of Surfactant-Free Copper Selenide Nanowires. *J. Colloid Interface Sci.* **2015**, *442*, 140−146.
(23) Sides, C. R.; Martin, C. R. Nanostructured Electrodes and the Low-Temperature Performance of Li-Ion Batteries. *Adv. Mater.* **2005**, *17*, 125−128.
(24) Nam, K. T.; Kim, D.-W.; Yoo, P. J.; Chiang, C.-Y.; Meethong, N.; Hammond, P. T.; Chiang, Y.-M.; Belcher, A. M. Virus-Enabled Synthesis and Assembly of Nanowires for Lithium Ion Battery Electrodes. *Science* **2006**, *312*, 885−888.
(25) Chan, C. K.; Peng, H.; Twesten, R. D.; Jarausch, K.; Zhang, X. F.; Cui, Y. Fast, Completely Reversible Li Insertion in Vanadium Pentoxide Nanoribbons. *Nano Lett.* **2007**, *7*, 490−495.
(26) Chen, D.; Chen, G.; Jin, R.; Xu, H. Self-Decorated $Cu_{2-x}Se$ Nanosheets as Anode Materials for Li Ion Batteries and Electrochemical Hydrogen Storage. *CrystEngComm* **2014**, *16*, 2810−2817.
(27) Jiang, J.; Li, H.; Huang, J.; Li, K.; Zeng, J.; Yang, Y.; Li, J.; Wang, Y.; Wang, J.; Zhao, J. Investigation of the Reversible Intercalation/Deintercalation of Al into the Novel Li_3VO_4@C Microsphere Composite Cathode Material for Aluminum-Ion Batteries. *ACS Appl. Mater. Interfaces* **2017**, *9*, 28486−28494.
(28) Yue, J.-L.; Sun, Q.; Fu, Z.-W. Cu_2Se with Facile Synthesis as a Cathode Material for Rechargeable Sodium Batteries. *Chem. Commun.* **2013**, *49*, 5868−5870.
(29) Li, H.; Wang, Y.; Huang, J.; Zhang, Y.; Zhao, J. Microwave-Assisted Synthesis of CuS/Graphene Composite for Enhanced Lithium Storage Properties. *Electrochim. Acta* **2017**, *225*, 443−451.
(30) Lee, B.; Lee, H. R.; Yim, T.; Kim, J. H.; Lee, J. G.; Chung, K. Y.; Cho, B. W.; Oh, S. H. Investigation on the Structural Evolutions during the Insertion of Aluminum Ions into Mo_6S_8 Chevrel Phase. *J. Electrochem. Soc.* **2016**, *163*, A1070−A1076.
(31) Sun, X.; Bonnick, P.; Duffort, V.; Liu, M.; Rong, Z.; Persson, K. A.; Ceder, G.; Nazar, L. F. A High Capacity Thiospinel Cathode for Mg Batteries. *Energy Environ. Sci.* **2016**, *9*, 2273−2277.
(32) Li, H.; Jiang, J.; Huang, J.; Wang, Y.; Peng, Y.; Zhang, Y.; Hwang, B.-J.; Zhao, J. Investigation of the Na Storage Property of One-Dimensional $Cu_{2-x}Se$ Nanorods. *ACS Appl. Mater. Interfaces* **2018**, *10*, 13491−13498.
(33) Li, H.; Wang, Y.; Jiang, J.; Zhang, Y.; Peng, Y.; Zhao, J. CuS Microspheres as High-Performance Anode Material for Na-ion Batteries. *Electrochim. Acta* **2017**, *247*, 851−859.
(34) Shaju, K. M.; Subba Rao, G. V.; Chowdari, B. V. R. Influence of Li-Ion Kinetics in the Cathodic Performance of Layered Li-$(Ni_{1/3}Co_{1/3}Mn_{1/3})O_2$. *J. Electrochem. Soc.* **2004**, *151*, A1324−A1332.
(35) Zhang, L.; Chen, L.; Luo, H.; Zhou, X.; Liu, Z. Large-Sized Few-Layer Graphene Enables an Ultrafast and Long-Life Aluminum-Ion Battery. *Adv. Energy Mater.* **2017**, *7*, 1700034.
(36) Akhavan, O.; Azimirad, R.; Safa, S.; Hasani, E. CuO/$Cu(OH)_2$ Hierarchical Nanostructures as Bactericidal Photocatalysts. *J. Mater. Chem.* **2011**, *21*, 9634−9640.
(37) Tahir, D.; Tougaard, S. Electronic and Optical Properties of Cu, CuO and Cu_2O Studied by Electron Spectroscopy. *J. Phys.: Condens. Matter* **2012**, *24*, 175002.
(38) Hayez, V.; Franquet, A.; Hubin, A.; Terryn, H. XPS Study of the Atmospheric Corrosion of Copper Alloys of Archaeological Interest. *Surf. Interface Anal.* **2004**, *36*, 876−879.
(39) Biesinger, M. C. Advanced Analysis of Copper X-Ray Photoelectron Spectra. *Surf. Interface Anal.* **2017**, *49*, 1325−1334.
(40) Liu, Y.-Y.; Wang, Z.-X.; He, X.; Shao, M.; Li, M.-X. One Unexpected Mixed-Valence Cu(I,II)-Cyanide Coordination Polymer In Situ Originating from the Cleavage of Acetonitrile. *Inorg. Chem. Commun.* **2017**, *80*, 46−48.
(41) Xu, J.; Zhang, W.; Yang, Z.; Ding, S.; Zeng, C.; Chen, L.; Wang, Q.; Yang, S. Large-Scale Synthesis of Long Crystalline $Cu_{2-x}Se$ Nanowire Bundles by Water-Evaporation-Induced Self-Assembly and Their Application in Gas Sensing. *Adv. Funct. Mater.* **2009**, *19*, 1759−1766.
(42) Sun, X.-G.; Fang, Y.; Jiang, X.; Yoshii, K.; Tsuda, T.; Dai, S. Polymer Gel Electrolytes for Application in Aluminum Deposition and Rechargeable Aluminum Ion Batteries. *Chem. Commun.* **2016**, *52*, 292−295.

DOI: 10.1021/acsami.8b03259
ACS Appl. Mater. Interfaces 2018, 10, 17942−17949